*Journal of The Electrochemical Society*, **155** (5) D408-D413 (2008)
0013-4651/2008/155(5)/D408/6/$23.00 © The Electrochemical Society

# In Situ Stress Measurements During Al UPD onto (111)-Textured Au from $AlCl_3$–EMImCl Ionic Liquid

**G. R. Stafford*,z and C. R. Beauchamp**

*Materials Science and Engineering Laboratory, National Institute of Standards and Technology, Gaithersburg, Maryland 20899, USA*

In situ stress measurements were made during Al underpotential deposition (upd) onto (111)-textured Au from Lewis acidic aluminum chloride, 1-ethyl-3-methylimidazolium chloride ($AlCl_3$–EMImCl), using the wafer curvature method. The surface stress response consists of three distinct features. In the potential range of 1.2–0.6 V the surface stress moves in the tensile (positive) direction from a value arbitrarily chosen as zero. This likely involves the desorption of $AlCl_4^-$ from the Au surface and is consistent with adsorbate-induced stress models that appear in the literature. At the start of Al upd, the surface stress moves in the compressive direction, in contrast to the tensile stress expected based on the positive lattice misfit. We attribute this compressive stress to the formation of Al–Au bonds which partially satisfy the bonding requirements of the Au surface atoms, thereby reducing the tensile surface stress inherent to the clean Au surface. In the latter stages of Al upd, the surface stress once again moves in the tensile direction, which we attribute to Al–Au alloying. The magnitude of the tensile stress change is close to that estimated from the elastic strain associated with the change in molar volume, using reaction kinetics reported for surface alloy formation in the upd region.

© 2008 The Electrochemical Society. [DOI: 10.1149/1.2894202] All rights reserved.

Manuscript submitted November 29, 2007; revised manuscript received February 8, 2008.
Available electronically March 20, 2008.

The underpotential deposition (upd) of metal monolayers onto foreign metal substrates is important to the electrodeposition community. In metal deposition involving Stranski–Krastanov nucleation and growth, the upd layer forms prior to the formation of three-dimensional (3-D) crystals so that an understanding of deposition processes in the upd region may help us better understand the growth and subsequent properties of bulk thin films. For this reason, upd processes have been extensively examined by in situ techniques such as electrochemical voltammetry/coulometry,[1-6] spectroscopy,[7-9] scanning probe microscopy,[10-15] X-ray scattering,[11,16,17] and quartz crystal nanogravimetry[18-20] in order to better understand the formation and structure of the upd adlayer.

An additional in situ probe gaining popularity in electrochemistry involves the measurement of surface and growth stress. Surface stress is the reversible work required to elastically deform a surface. The loss of bonds at a clean metal surface causes a redistribution of charge density between the remaining surface atoms, thereby increasing their attractive interaction and causing a decrease in their equilibrium interatomic spacing. Because the surface atoms are held in place by the bulk lattice, they are stretched from their equilibrium lattice positions and a surface stress arises. The sign of the surface stress is positive (tensile) if the surface would like to contract under its own stress. The adsorption of species on the surface can be expected to alter the surface stress, because the local interaction of each adsorbate alters the bond strength between neighboring atoms on the surface. The sensitivity of surface stress to both ionic and fully discharged adsorbates such as metal monolayers makes this measurement particularly relevant for upd studies, where both processes tend to occur simultaneously. For instance, in the case of Pb upd onto (111)-textured Au in $HClO_4$ supporting electrolyte, the stress transient clearly shows regions of $ClO_4^-$ desorption, Pb–Au bond formation, stress relaxation due to island coalescence, and compression of the monolayer at potentials just positive of bulk Pb deposition.[21,22]

It is readily apparent from experimental data reported in the literature that the surface stress change following growth of a pseudomorphic $(1 \times 1)$ metal monolayer cannot be estimated from continuum elasticity theory using the difference between the bulk lattice parameters to determine a misfit strain. When the misfit is positive (small adsorbate), elasticity theory predicts a tensile stress; however, there are several examples where the opposite is true, namely the upd of Cu on Au(111)[23-27] and the vapor deposition of Fe on W(110).[28] As expected, when the misfit is negative (large adsorbate), elasticity theory predicts compressive stress which is generally supported by experiment, although there is some discrepancy regarding the magnitude of the compressive stress.[29,30]

The various thermodynamic contributions for an epitaxial bilayer have been described by Cammarata et al.,[31,32] where the surface stress change includes contributions from the substrate–adlayer interface, the adlayer surface, and the lattice misfit between the metal adlayer and the substrate. This has been used to obtain the critical thickness associated with the loss of coherency for thin-film epitaxy.[32] A similar treatment has been extended to epitaxial systems formed electrochemically where an electrocapillary correction is added to account for the change in the point of zero charge (pzc) with the addition of the adlayer.[26,33] Wafer-curvature experiments have been conducted on a variety of upd systems, namely, $Pb^{2+}$/Au(111), $Pb^{2+}$/Ag(111), and $Ag^+$/Au(111), and the measured stress changes were used to estimate the interface stress of the substrate/adlayer interface. A similar treatment has been applied to the Cu/Au(111) system where the contribution of anion adsorption was considered as well.[26,33] It is not clear whether use of an epitaxial bilayer model, where both film and substrate are considered to have bulklike properties, properly describes upd where the adlayer is restricted to a monolayer.

Leiva et al. have used the embedded-atom method to calculate the surface stress due to epitaxial monolayer adsorption for a variety of face-centered cubic adsorbate–substrate combinations.[34] When adsorption energy is considered together with lattice misfit, they find qualitative agreement with experimental data. The adsorption contribution is particularly apparent for systems with positive misfit (small adsorbate), such as Cu on Au. The embedded-atom calculation predicts compressive stress, consistent with experimental data,[23,25-27] whereas considering the +12.8% misfit alone leads to tensile stress. Leiva et al. have further shown that the adsorption-energy contribution of the monolayer to the change in surface stress is negative for all of the adsorbate–substrate combinations examined.[34] The surface stress change is then a balance between an adsorption contribution which is negative and a misfit term which can be positive or negative.

Because upd is at least partially driven by the free energy of dissimilar bonding, one would always expect the adsorption contribution to favor compressive stress. In addition, because upd processes often result in a negative shift of the pzc, anion readsorption onto the newly formed adlayer generally results in an additional compressive contribution to the surface stress, similar to that observed for Cu/Au(111).[23-27] One is then left to question how significant the lattice misfit contribution is toward the surface stress

* Electrochemical Society Active Member.
z E-mail: gery.stafford@nist.gov

change during upd processes. One could argue that in the case of Cu/Au(111), the lattice misfit is too large to make a meaningful contribution to the stress. Obtaining surface stress data on other upd systems that have a positive but smaller lattice mismatch, such as Pd/Au(111) (+4.9% mismatch)[35] or Al/Au(111) (+0.7% mismatch), might facilitate the discussion. In a previous paper, we examined the growth stress associated with Al deposition on (111)-textured Au, a process described by Stranski–Krastanov 3-D growth.[36] In that paper we briefly described the upd of Al on both (111)-textured Cu and (111)-textured Au cantilever electrodes and noted some anomalous behavior in the case of Al–Au. The purpose of this paper is to examine the surface stress changes associated with Al upd on (111)-textured Au in more detail, paying particular attention to differentiating the stress behavior attributed to Al monolayer formation and Al–Au alloy formation in the upd region.

The electrodeposition of aluminum must be carried out from nonaqueous or aprotic solvents, because hydrogen is evolved in aqueous solutions before aluminum can be deposited. The direct electrodeposition of aluminum from ambient-temperature ionic liquids has received considerable attention. These electrolytes are prepared by combining $AlCl_3$ with certain unsymmetrical quaternary ammonium chloride salts such as 1-ethyl-3-methylimidazolium chloride (EMImCl).[37] They are liquid at room temperature and display adjustable Lewis acidity. Melts prepared with a molar excess of $AlCl_3$ (>50% mole fraction $AlCl_3$) are Lewis acidic due to the presence of the coordinately unsaturated $Al_2Cl_7^-$ ion, whereas those formulated with a molar excess of the quaternary ammonium chloride salt (<50% mole fraction $AlCl_3$) are termed Lewis basic because they contain a chloride ion that is not covalently bound to aluminum. The cathodic limit of the acidic $AlCl_3$–EMImCl melts is governed by the electrodeposition of aluminum according to the following reaction

$$4Al_2Cl_7^- + 3e^- \rightarrow Al + 7AlCl_4^- \quad [1]$$

Aluminum cannot be electrodeposited from basic melts due to the preferential reduction of the 1-ethyl-3-methylimidazolium cation over $AlCl_4^-$. Numerous reports describing the electrodeposition of aluminum and its alloys from the Lewis acidic $AlCl_3$–EMImCl ionic liquids appear in the literature.[38-41] Recently it has been shown that aluminum can be electrodeposited from the new generation of air- and water-stable ionic liquids following controlled addition of $AlCl_3$.[42,43]

## Experimental

In situ stress measurements were made on an optical bench using the wafer-curvature method.[21,25] The cantilever was a borosilicate glass strip (D 263, Schott) measuring $60 \times 3 \times 0.108$ mm. The glass had a Young's modulus of $72.9 \times 10^9$ N m$^{-2}$ and a Poisson ratio of 0.208, as specified by the vendor. Onto one side of the cantilever a 4 nm thick adhesion layer of titanium and a subsequent 250 nm film of gold were vapor-deposited by electron-beam evaporation. The glass–metal interface provided the reflective surface for the laser beam. Prior to use, the electrodes were cleaned in piranha solution (3:1 volume mixture of concentrated $H_2SO_4$:30% $H_2O_2$). The Au electrodes had a strong (111) crystallographic orientation. The 200 reflection was not apparent in θ–2θ X-ray scans, and rocking curves of the 111 reflection generally yielded a full width at half-maximum on the order of 2°. These films have a fiber texture, i.e., there is no in-plane orientation. Field-emission scanning electron microscopy shows the Au grain size to be on the order of 25 nm. The curvature of the substrate was monitored while under potential control by reflecting a HeNe laser off of the glass/metal interface onto a position-sensitive detector. The relationship between the surface stress and the radius of curvature of the cantilever is given by Stoney's equation.[44]

The electrochemical cell was an air-tight single-compartment Pyrex cell. A glass disk was joined to the back of the cell to allow the cell to be held and positioned by a standard mirror mount on the optical bench. The electrolyte was a 55:45 mole ratio of $AlCl_3$–EMImCl. It was prepared and purified using the procedures outlined in Ref. 37. The counter electrode was an aluminum wire placed parallel to and in the same solution as the working electrode. The reference electrode was also an aluminum wire placed in the same solution as the working electrode and positioned between the working and counter electrodes. All potentials reported here are with respect to the Al reference. The electrolyte was added to the cell while in a dry box containing less than 2 ppm oxygen and was then sealed. The cell was then removed from the dry box, placed in the optical mount, and positioned on the optical bench. Potential control was maintained using an EG&G Princeton Applied Research Corp. model 273 potentiostat/galvanostat that was controlled by a Dell Pentium 4 computer and LabView software. A more-detailed description of the optical bench and stress measurement can be found in Ref. 25 and 36.

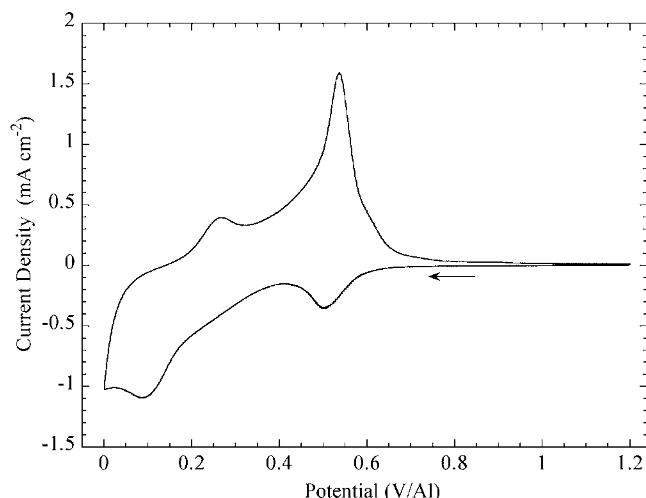


**Figure 1.** Linear sweep voltammetry associated with the upd of Al onto (111)-textured Au in 55:45 mole ratio of $AlCl_3$-EMImCl. Sweep rate was 20 mV s$^{-1}$.

## Results and Discussion

Figure 1 shows the linear sweep voltammetry for the upd of Al onto (111)-textured Au from a 55:45 mole ratio of $AlCl_3$-EMImCl electrolyte. The voltammetry shows two cathodic peaks at 0.5 and 0.1 V as well as two anodic peaks at 0.26 and 0.54 V. This voltammetry is similar to that reported by Lee et al. on polycrystalline Au in 60:40 mole ratio of $AlCl_3$-EMImCl.[45] Reports in the literature indicate that Al–Au alloys can be formed in the upd region.[45-48] The general consensus is that stripping of the upd layer occurs in the potential range of 0.4–0.6 V and that the first anodic peak is associated with dealloying rather than partial removal of the upd layer. This conclusion is based on the fact that the height of the first oxidation wave increases with the time at which the electrode is held at +0.10 V.[45] Zell et al. have shown by in situ scanning tunneling microscopy (STM) that in the potential region of 0.2–0.4 V two-dimensional (2-D) aluminum clusters measuring 1–2 nm in diameter are deposited on the bare Au surface.[48] When the potential is further decreased to 0.1 V, the number of 2-D clusters increases and 3-D growth is observed. When the Al is anodically removed at 1.1 V, holes are left in the Au surface, indicating that surface alloying and perhaps compound formation occur in the upd region.[48] Similar surface alloying has been reported for evaporated Al on Au(111) at and below room temperature.[49]

We first examine the upd process by limiting the cathodic potential to +0.3 V in order to avoid significant alloy formation. Figure 2 shows the voltammetry (a) and surface stress response (b) for sweep rates ranging from 10 to 500 mV s$^{-1}$ from a starting potential of

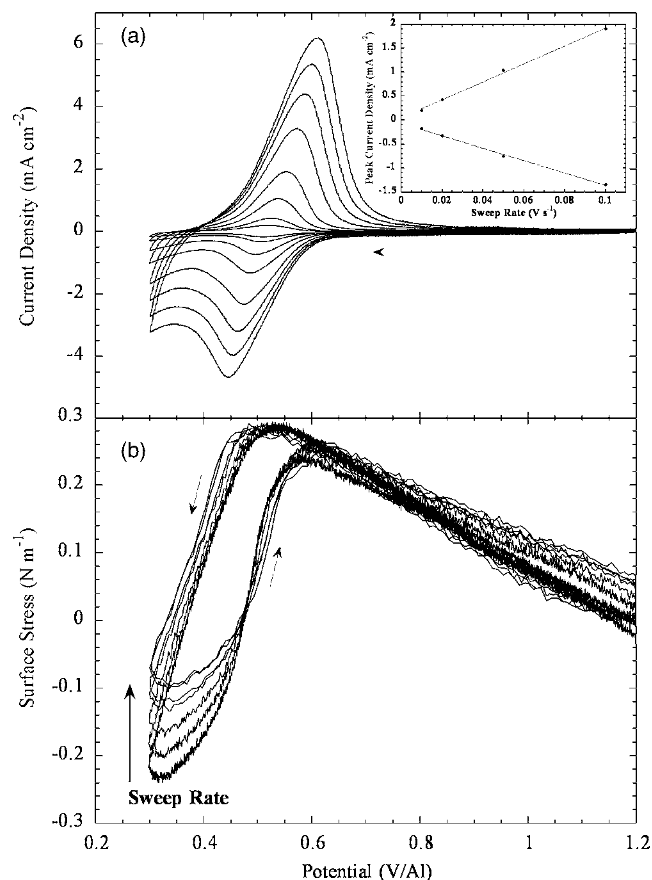


**Figure 2.** (a) Linear sweep voltammetry and (b) surface stress response for the upd of Al (limited to the first voltammetric wave) onto (111)-textured Au in 55:45 mole ratio of $AlCl_3$-EMImCl. Sweep rate was varied from 10 to 500 mV $s^{-1}$. The inset in (a) shows the peak current density for both deposition and stripping as a function of sweep rate.

1.2 V. The voltammetric waves appear to be quasi-reversible, based on the sweep-rate dependence of the peak potential.[50] The inset shows that the peak current density, for both cathodic and anodic processes, varies linearly with sweep rate, indicating a surface-limited process. The charge is estimated to be about 1.8 mC $cm^{-2}$, which is approximately a factor of 2.5 higher than the 0.67 mC $cm^{-2}$ expected for a pseudomorphic monolayer of Al on Au(111). A typical roughness factor for the as-evaporated Au cantilever is 1.3, based on the charge necessary to completely reduce the Au oxide in acidic aqueous electrolyte.[51] The higher roughness factor, as determined from the Al upd charge, suggests that cycling the electrode in the upd region causes additional roughness due to the formation and removal of the surface alloy.

The surface stress response for Al upd is shown in Fig. 2b. In the potential range of +1.2 to + 0.55 V the surface stress moves in the tensile (positive) direction from a value arbitrarily chosen as zero. The stress response is likely due to both electrocapillarity as well as the desorption of $AlCl_4^-$ from the gold surface. An ordered adlayer of $AlCl_4^-$ has been observed by STM at potentials positive of Al upd on both Cu(111) in 55:45 mole ratio $AlCl_3$-EMImCl electrolyte[52] and Au(111) in 58:42 mole ratio $AlCl_3$-1-butyl-3-methylimidazolium chloride.[53] The tensile stress change in response to the desorption is consistent with Ibach's surface-induced charge-redistribution model, where electron acceptors such as adsorbed anions cause compressive stress because they reduce the electron density in the surface.[54] Haiss has observed a linear correlation between surface stress and surface charge for the adsorption/desorption of a variety of anions on Au.[55] In the potential range of +0.55 to + 0.30 V, corresponding to the onset of Al upd in Fig. 2a, the surface stress moves in the compressive direction. The stress maximum occurs well into the upd region, suggesting that perhaps two competing processes, i.e., $AlCl_4^-$ desorption and Al upd, occur simultaneously in the early stages of adlayer formation. Similar behavior has been observed for Bi and Pb upd on Au.[21,22] The magnitude of the compressive stress at the +0.3 V cathodic limit is a function of sweep rate, indicating some kinetic limitations in the stress response. When the potential scan is reversed, the stress response for the return sweep follows a path similar to that of the forward scan, although significant hysteresis is present in the deposition region, reflecting the quasi-reversibility of the voltammetry.

As mentioned previously, Al has a positive misfit (0.74%) with respect to the Au substrate. As a consequence, one would expect a tensile stress change for a pseudomorphic $(1 \times 1)$ adlayer considering misfit alone. This can be quantified by the following expression[56]

$$\tau = \frac{Y_{(111)}}{1 - \nu_{(111)}} \varepsilon_{\mathrm{mf}} d_{(111)} \theta \qquad [2]$$

where $Y_{(111)}$ is Young's modulus for the (111) surface of Al, $\nu_{(111)}$ is the Poisson ratio, $\varepsilon_{\mathrm{mf}}$ is the misfit strain, $d_{(111)}$ is the height of the monolayer, and $\theta$ is the number of monolayers on the surface. The elastic constants, calculated from the elastic compliances for Al,[57] are $Y_{(111)} = 72$ GPa and $\nu_{(111)} = 0.365$. Inserting these values into Eq. 2 for a monolayer of aluminum results in a misfit stress of +0.24 N $m^{-1}$. It is clear from Fig. 2 that the upd of Al results in a compressive stress rather than the tensile stress predicted from lattice misfit.

We now examine the stress response for more cathodic potentials where surface alloys are known to form in the upd region. These transients are shown in Fig. 3 for a variety of cathodic limits extending down to 0 V. If the cathodic limit does not go negative of +0.2 V, then the stress response is identical to that shown in Fig. 2b and the cantilever position returns to its initial zero value at the completion of the transient. As the potential is reduced to less than +0.15 V, the stress begins to move in the tensile direction. The stress continues to increase on the return sweep until the first anodic wave occurs, after which the stress returns to a value somewhat higher than its initial value. However, the cantilever returns to its original position if left for several minutes at a potential of 1.2 V. We attribute this tensile transient and remnant tensile stress at 1.2 V to Al–Au surface alloying.

In order to examine the kinetics of stress evolution, potential-step experiments were conducted to complement the potentiodynamic scans of Fig. 3. Selected transients are shown in Fig. 4a for pulses initiated at 1.2 V. When the potential is stepped to values positive of Al upd (+0.6 V), the stress change in the tensile direction is rapid and the stress remains constant for the 20 s duration of the pulse. The change in surface stress in this potential region is due to electrocapillarity and $AlCl_4^-$ desorption; both of these processes are expected to be rapid, which explains the shape of the transient in Fig. 4a. When the potential is pulsed into the upd region but positive of alloy formation (+0.2 V), the stress first moves in the tensile direction, reflecting $AlCl_4^-$ desorption, and then moves compressively as the Al monolayer forms on the Au. The compressive stress change due to Al upd is rather slow, which is consistent with the sweep-rate dependence of the stress response in Fig. 2b. The total stress change with respect to the clean Au surface at +0.6 V is approximately −0.9 N $m^{-1}$. When the potential is stepped more cathodically into the region of alloy formation, the stress follows the same progression, i.e., rapid tensile for $AlCl_4^-$ desorption, compressive for Al upd, followed by a second tensile transient. When the potential is pulsed to more cathodic potentials, it becomes clear that the time constant for the second tensile transient is potential dependent. The potential-step data is summarized in Fig. 4b, where the stress change, recorded after 20 s, for both the cathodic and anodic pulses is plotted

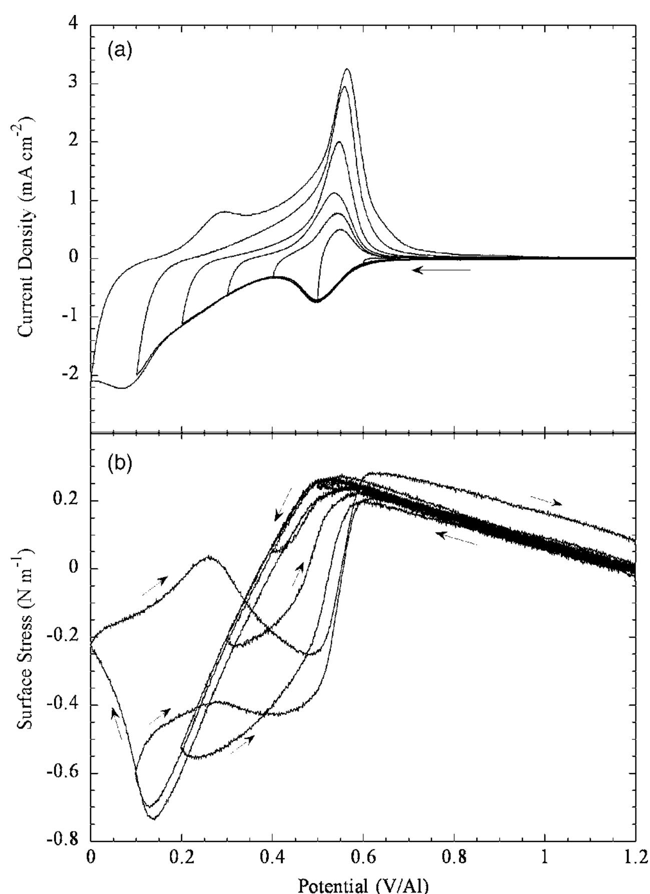


**Figure 3.** (a) Linear sweep voltammetry and (b) surface stress response for the upd of Al onto (111)-textured Au in 55:45 mole ratio of $AlCl_3$-EMImCl. The starting potential was +1.2 V while the cathodic limit was varied from +0.6 to 0 V. Sweep rate was 50 mV s$^{-1}$.

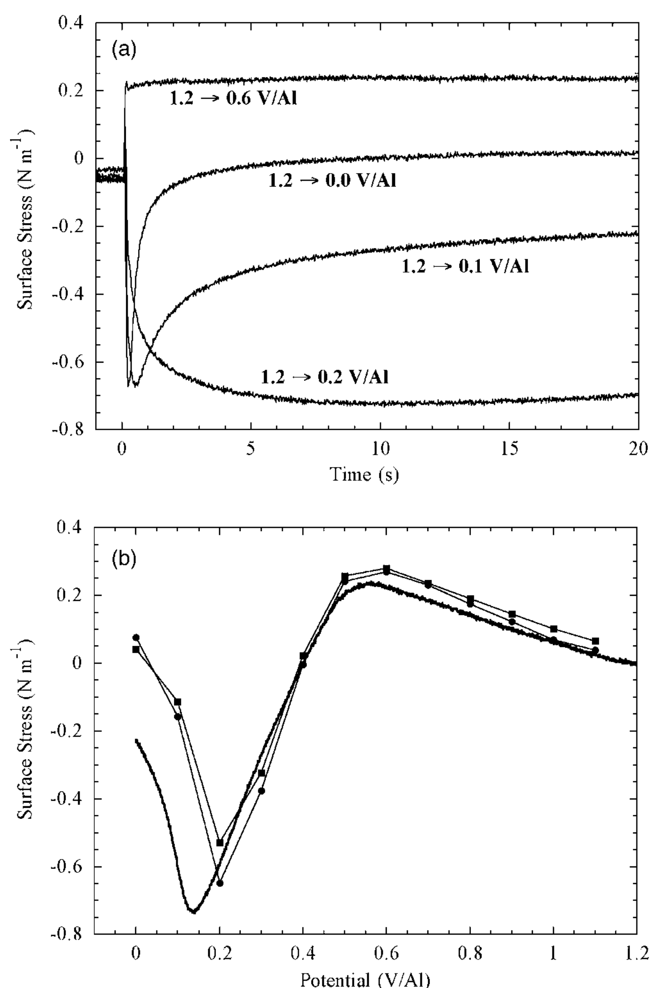


**Figure 4.** (a) Surface stress-time transients for the upd of Al onto (111)-textured Au in 55:45 mole ratio of $AlCl_3$-EMImCl in response to the cathodic potential steps indicated in the figure. (b) Stress change as a function of step potential, recorded after 20 s, for the cathodic step (—●—) and the return anodic step to 1.2 V (—■—). Potentiodynamic scan recorded at a sweep rate of 50 mV s$^{-1}$ (—).

as a function of step potential. For comparison, a potentiodynamic scan using a sweep rate of 50 mV s$^{-1}$ is also plotted. The agreement is excellent for both the $AlCl_4^-$ desorption and Al monolayer regions, whereas the stress response for the potentiodynamic scan slightly lags behind the potential step response in the surface alloy region.

The stress transients shown in Fig. 4b consist of three distinct features. The tensile stress observed at positive potentials (1.2–0.6 V) that we ascribe to $AlCl_4^-$ desorption as well as the compressive stress associated with Al monolayer formation are common features of stress transients reported in the literature for a variety of upd processes. However, the potential-dependent tensile transient observed in the latter stages of Al upd (0.15–0.0 V) is quite unusual and warrants additional discussion. Stress arises when a film undergoes any dynamic microstructural evolution process that changes its density while rigidly attached to the substrate. Tensile stress generated during film growth is an indication that the density of the film is increasing, i.e., there is a net decrease in molar volume. The initial stages of alloy formation in the upd region involve place-exchange processes between the Al adlayer and surface Au atoms. The stress response to replacing some of the surface Au atoms with smaller Al atoms can be estimated using an expression similar to Eq. 2

$$\tau = E'_{111}\varepsilon_{\mathrm{mf}}d_{(111)}\theta_{\mathrm{e}} \qquad [3]$$

where $E'_{111}$ is the biaxial modulus for the (111) surface of Au [i.e., $Y_{(111)}/(1-\nu_{(111)})$], $\varepsilon_{\mathrm{mf}}$ is the +0.74% misfit strain between Al and Au, $d_{(111)}$ is the height of the Au surface layer, and $\theta_{\mathrm{e}}$ is the fraction of the Au surface that has been exchanged by Al atoms. The biaxial modulus, calculated from the elastic compliances for Au,[57] is 190.3 GPa. If we arbitrarily allow 10% of the surface Au atoms to be replaced by Al, then the tensile stress generated in the Au–Al alloy surface layer is +0.04 N m$^{-1}$, only a fraction of that measured experimentally. This is a clear indication that the decrease in molar volume of the surface alloy layer must be more substantial than that described by a simple place exchange of Al and Au atoms on the surface.

STM studies of surface alloying of evaporated Al on Au(111) at room temperature have shown lattice contractions in the surface alloy that are unusually large in light of the similar atomic radii of Al and Au.[49] It is also well known that large negative deviations from a rule of mixtures addition of the constituent molar volumes exist in several binary Al-transition-metal alloys. The high lattice contraction of the Al–Au surface alloy observed by STM is then rationalized as the 2-D analogue of the Al atom contraction in the binary bulk alloys.[49] For example, the molar volume contraction, $\Delta V/V$, associated with the formation of orthorhombic $AlAu_2$ is −0.056. The stress change associated with bulk alloy formation can then be estimated from the molar volume contraction

$$\tau_{\mathrm{imc}} = -E'_{\mathrm{imc}}\frac{\Delta V}{3V}d_{\mathrm{imc}} \qquad [4]$$

where $E'_{\mathrm{imc}}$ is the biaxial modulus of the intermetallic and $d_{\mathrm{imc}}$ is the intermetallic thickness. If one assumes an $E'_{\mathrm{imc}}$ of 200 GPa and in-

cludes the $\Delta V/V$ of $-0.056$, then the volume contraction due to surface alloying produces a stress change of $+3.7$ N $m^{-1}$ for each nm of intermetallic formed. Lattice contractions of this magnitude can certainly explain the tensile-stress changes observed experimentally.

We now examine the kinetics of surface alloy formation. The stress transients in Fig. 4a indicate that both the time constant and the magnitude of the alloy-induced tensile stress are potential-dependent. Similar potential dependence for alloy formation in the upd region has been observed for Cd on Ag.[58] Specifically, the logarithm of the rate constant was found to increase linearly as the potential was made more negative, approaching the bulk deposition of Cd. This was attributed to a Nernst-type dependence of the Cd activity at the surface on electrode potential. Garcia et al. have further characterized the Cd–Ag system by STM.[59] A thin surface alloy film forms as the result of structural changes in the full monolayer that are initiated by place-exchange processes between the Cd adlayer and surface Ag atoms. An effective diffusion coefficient of $1.5 \times 10^{-16}$ $cm^2$ $s^{-1}$ was obtained from charge-time transients using an alloying potential of $+10$ mV with respect to bulk Cd. Based on these kinetics, one can expect a Cd–Ag surface alloy measuring approximately 0.5 nm in thickness to form after 20 s at room temperature.

The Cd–Ag data cited above suggests that the kinetics of alloy formation in the upd region is sufficient to cause the stress transients shown in Fig. 4. Although similar room-temperature data is not available for the formation of Al–Au alloys in the upd region, this system has been examined in some detail at higher temperatures in $AlCl_3$–NaCl electrolyte.[47] The presence of both $AlAu_2$ and $Al_2Au_5$ has been confirmed after 2 h at 250°C. An Arrhenius plot of the high-temperature data suggests that at 25°C, an Al–Au diffusion zone of 0.27 nm forms after 60 s. This is in reasonable agreement with the ambient-temperature surface alloy kinetics described above for Cd–Ag. Phase-formation studies on Al–Au thin films have shown that both $Al_2Au_5$ and $AlAu_2$ also form at room temperature.[60] Based on the molar volume-induced stress change described by Eq. 4, the 0.27 nm of $AlAu_2$ formed in 60 s, estimated from the high-temperature kinetic data, would result in a surface stress of $+1.0$ N $m^{-1}$, which is in the same range as that observed experimentally. Although these kinetic studies suggest that surface alloying may be responsible for the tensile stress observed in the latter stages of Al upd on Au, the kinetics of Al–Au alloy formation at room temperature, as well as the stress changes associated with this process, will have to be evaluated more thoroughly.

## Conclusion

In situ stress measurements were made during Al upd onto (111)-textured Au from Lewis acidic $AlCl_3$-EMImCl using the wafer-curvature method. The surface stress response consists of three distinct features. In the potential range of 1.2–0.6 V the surface stress moves in the tensile (positive) direction from a value arbitrarily chosen as zero. This likely involves the desorption of $AlCl_4^-$ from the Au surface and is consistent with adsorbate-induced stress models that appear in the literature. At the start of Al upd, the surface stress moves in the compressive direction, in contrast to the tensile stress expected based on the positive lattice misfit. We attribute this compressive stress to the formation of Al–Au bonds which partially satisfy the bonding requirements of the Au surface atoms, thereby reducing the tensile surface stress inherent to the clean Au surface. In the latter stages of Al upd, the surface stress once again moves in the tensile direction, which we attribute to Al–Au alloying. The magnitude of the tensile-stress change is close to that estimated from the elastic strain associated with the change in molar volume, using reaction kinetics reported for surface alloy formation in the upd region.

## Acknowledgments

The authors gratefully acknowledge the technical contributions of Charles Hussey, Ugo Bertocci, Thomas Moffat, Jonathon Guyer, and Ole Kongstein. We are particularly grateful to Tetsuya Tsuda and Charles Hussey for providing the $AlCl_3$-EMImCl.

*National Institute of Standards and Technology assisted in meeting the publication costs of this article.*

## References

1. A. Hamelin, *J. Electroanal. Chem. Interfacial Electrochem.*, **165**, 167 (1984).
2. A. Hamelin and J. Lipkowski, *J. Electroanal. Chem. Interfacial Electrochem.*, **171**, 317 (1984).
3. E. Kirowa-Eisner, Y. Bonfil, D. Tzur, and E. Gileadi, *J. Electroanal. Chem.*, **552**, 171 (2003).
4. B. K. Niece and A. A. Gewirth, *Langmuir*, **12**, 4909 (1996).
5. S. Sayed and K. Juttner, *Electrochim. Acta*, **28**, 1635 (1983).
6. T. Solomun and W. Kautek, *Electrochim. Acta*, **47**, 679 (2001).
7. R. Adzic, V. Jovancicevic, and M. Podlavicky, *Electrochim. Acta*, **25**, 1143 (1980).
8. R. Adzic, E. Yeager, and B. D. Cahan, *J. Electrochem. Soc.*, **121**, 474 (1974).
9. M. Futamata, *Chem. Phys. Lett.*, **333**, 337 (2001).
10. C.-H. Chen and A. Gewirth, *J. Am. Chem. Soc.*, **114**, 5439 (1992).
11. C.-H. Chen, K. D. Kepler, A. A. Gewirth, B. M. Ocko, and J. Wang, *J. Phys. Chem.*, **97**, 7290 (1993).
12. C.-H. Chen, N. Washburn, and A. A. Gewirth, *J. Phys. Chem.*, **97**, 9754 (1993).
13. M. Hara, Y. Nagahara, J. Inukai, S. Yoshimoto, and K. Itaya, *Electrochim. Acta*, **51**, 2327 (2006).
14. C. A. Jeffrey, D. A. Harrington, and S. Morin, *Surf. Sci.*, **512**, L367 (2002).
15. N. J. Tao, J. Pan, Y. Li, P. I. Oden, J. A. DeRose, and S. M. Lindsay, *Surf. Sci. Lett.*, **271**, L338 (1992).
16. K. Tamura, J. Wang, R. Adzic, and B. Ocko, *J. Phys. Chem. B*, **108**, 1992 (2004).
17. M. F. Toney, J. N. Howard, J. Richer, G. L. Borges, J. G. Gordon, O. R. Melroy, D. Yee, and L. B. Sorenson, *Phys. Rev. Lett.*, **75**, 4472 (1995).
18. M. R. Deakin and O. R. Melroy, *J. Electroanal. Chem. Interfacial Electrochem.*, **239**, 321 (1988).
19. M. Hepel, K. Kanige, and S. Bruckenstein, *Langmuir*, **6**, 1063 (1990).
20. O. Melroy, K. Kanazawa, J. G. G. Gordon II, and D. Buttry, *Langmuir*, **2**, 697 (1986).
21. G. R. Stafford and U. Bertocci, *J. Phys. Chem. B*, **110**, 15493 (2006).
22. G. R. Stafford and U. Bertocci, *J. Phys. Chem. C*, **111**, 17580 (2007).
23. W. Haiss and J. K. Sass, *J. Electroanal. Chem.*, **386**, 267 (1995).
24. W. Haiss, R. J. Nichols, and J. K. Sass, *Surf. Sci.*, **388**, 141 (1997).
25. O. E. Kongstein, U. Bertocci, and G. R. Stafford, *J. Electrochem. Soc.*, **152**, C116 (2005).
26. T. Trimble, L. Tang, N. Vasiljevic, N. Dimitrov, M. van Schilfgaarde, C. Friesen, C. V. Thompson, S. C. Seel, J. A. Floro, and K. Sieradzki, *Phys. Rev. Lett.*, **95**, 166106 (2005).
27. M. Seo and M. Yamazaki, *J. Solid State Electrochem.*, **11**, 1365 (2007).
28. H. L. Meyerheim, D. Sander, R. Popescu, and J. Kirschner, *Phys. Rev. B*, **64**, 045414 (2001).
29. T. A. Brunt, E. D. Chabala, T. Rayment, S. J. O'shea, and M. E. Welland, *J. Chem. Soc., Faraday Trans.*, **92**, 3807 (1996).
30. A. Grossmann, W. Erley, J. B. Hannon, and H. Ibach, *Phys. Rev. Lett.*, **77**, 127 (1996).
31. R. C. Cammarata and K. Sieradzki, *Annu. Rev. Mater. Sci.*, **24**, 215 (1994).
32. R. C. Cammarata, K. Sieradzki, and F. Spaepen, *J. Appl. Phys.*, **87**, 1227 (2000).
33. C. Friesen, N. Dimitrov, R. C. Cammarata, and K. Sieradzki, *Langmuir*, **17**, 807 (2001).
34. E. P. M. Leiva, M. G. Del Popolo, and W. Schmickler, *Chem. Phys. Lett.*, **320**, 393 (2000).
35. L. A. Kibler, M. Kleinert, R. Randler, and D. M. Kolb, *Surf. Sci.*, **443**, 19 (1999).
36. G. R. Stafford, O. E. Kongstein, and G. M. Haarberg, *J. Electrochem. Soc.*, **153**, C207 (2006).
37. J. S. Wilkes, J. A. Levisky, R. A. Wilson, and C. L. Hussey, *Inorg. Chem.*, **21**, 1263 (1982).
38. R. T. Carlin, W. Crawford, and M. Bersch, *J. Electrochem. Soc.*, **139**, 2720 (1992).
39. Q. Liao, W. R. Pitner, G. Stewart, C. L. Hussey, and G. R. Stafford, *J. Electrochem. Soc.*, **144**, 936 (1997).
40. J. Robinson and R. A. Osteryoung, *J. Electrochem. Soc.*, **127**, 122 (1980).
41. G. R. Stafford and C. L. Hussey, *Advances in Electrochemical Science and Engineering*, Vol. 7, R. C. Alkire and D. M. Kolb, Editors, Wiley-VCH, Weinheim, Germany (2002).
42. S. Z. El Abedin, E. M. Moustafa, R. Hempelmann, H. Natter, and F. Endres, *ChemPhysChem*, **7**, 1535 (2006).
43. E. M. Moustafa, S. Z. El Abedin, A. Shkurankov, E. Zschippang, A. Y. Saad, A. Bund, and F. Endres, *J. Phys. Chem. B*, **111**, 4693 (2007).
44. G. G. Stoney, *Proc. R. Soc. London, Ser. A*, **82**, 172 (1909).
45. J.-J. Lee, I. T. Bae, D. A. Scherson, B. Miller, and K. A. Wheeler, *J. Electrochem. Soc.*, **147**, 562 (2000).
46. J.-J. Lee, Y. Mo, D. A. Scherson, B. Miller, and K. A. Wheeler, *J. Electrochem. Soc.*, **148**, C799 (2001).
47. B. S. Radovic, R. A. H. Edwards, and J. N. Jovicevic, *J. Electroanal. Chem.*, **428**, 113 (1997).
48. C. A. Zell, F. Endres, and W. Freyland, *Phys. Chem. Chem. Phys.*, **1**, 697 (1999).
49. B. Fischer, J. V. Barth, A. Fricke, L. Nedelmann, and K. Kern, *Surf. Sci.*, **389**, 366 (1997).
50. A. J. Bard and L. R. Faulkner, *Electrochemical Methods: Fundamentals and Applications*, John Wiley and Sons, New York (1980).

51. S. Trasatti and O. A. Petrii, *Pure Appl. Chem.*, **63**, 711 (1991).
52. G. R. Stafford, V. D. Jovic, T. P. Moffat, Q. Zhu, S. Jones, and C. L. Hussey, in *Molten Salts*, PV 99-41, p. 535, The Electrochemical Society Proceeding Series, Pennington, NJ (1999).
53. O. Mann and W. Freyland, *J. Phys. Chem. C*, **111**, 9832 (2007).
54. H. Ibach, *J. Vac. Sci. Technol. A*, **A12**, 2240 (1994).
55. W. Haiss, R. J. Nichols, J. K. Sass, and K. P. Charle, *J. Electroanal. Chem.*, **452**, 199 (1998).
56. H. Ibach, *Surf. Sci. Rep.*, **29**, 193 (1997).
57. G. Simmons and H. Wang, *Single Crystal Elastic Constants and Calculated Aggregate Properties: A Handbook*, MIT Press, Cambridge, MA (1971).
58. H. Bort, K. Juttner, W. J. Lorenz, and G. Staikov, *Electrochim. Acta*, **28**, 993 (1983).
59. S. G. Garcia, D. R. Salinas, and G. Staikov, *Surf. Sci.*, **576**, 9 (2005).
60. G. Majni, C. Nobili, G. Ottaviana, M. Costato, and E. Galli, *J. Appl. Phys.*, **52**, 4047 (1981).